Enhanced Phase-Sensitive SSFP Reconstruction for Fat-Water Separation in Phased-Array Acquisitions

Ozgur Yilmaz, BS,[1,2] Emine Ulku Saritas, PhD,[1,2,3] and Tolga Çukur, PhD[1,2,3]*

Purpose: To propose and assess a method to improve the reliability of phase-sensitive fat–water separation for phased-array balanced steady-state free precession (bSSFP) acquisitions. Phase-sensitive steady-state free precession (PS-SSFP) is an efficient fat–water separation technique that detects the phase difference between neighboring bands in the bSSFP magnetization profile. However, large spatial variations in the sensitivity profiles of phased-array coils can lead to noisy phase estimates away from the coil centers, compromising tissue classification.

Materials and Methods: We first perform region-growing phase correction in individual coil images via unsupervised selection of a fat-voxel seed near the peak of each coil's sensitivity profile. We then use an optimal linear combination of phase-corrected images to segregate fat and water signals. The proposed method was demonstrated on noncontrast-enhanced SSFP angiograms of the thigh, lower leg, and foot acquired at 1.5T using an 8-channel coil. Individual coil PS-SSFP with a common seed selection for all coils, individual coil PS-SSFP with coil-wise seed selection, PS-SSFP after coil combination, and IDEAL reconstructions were also performed. Water images reconstructed via PS-SSFP methods were compared in terms of the level of fat suppression and the similarity to reference IDEAL images (signed-rank test).

Results: While tissue misclassification was broadly evident across regular PS-SSFP images, the proposed method achieved significantly higher levels of fat suppression ($P < 0.005$) and increased similarity to reference IDEAL images ($P < 0.005$).

Conclusion: The proposed method enhances fat–water separation in phased-array acquisitions by producing improved phase estimates across the imaging volume.

J. MAGN. RESON. IMAGING 2016;44:148–157.

Balanced Steady-State Free Precession (bSSFP) sequences typically generate relatively higher levels of signal from fat when compared to water tissues. However, separation of these two resonances is critical for many applications including cartilage imaging,[1] abdominal imaging,[2] and angiography.[3,4] Among the approaches proposed to address this problem were steady-state techniques that reshape magnetization profiles,[5–7] techniques that temporarily alter transient signal profiles,[8–10] and Dixon-type techniques that rely on multiple acquisitions to separate the two resonances.[11–14] Because the above techniques either suppress fat signals during acquisition or perform subvoxel fat–water decomposition based on multiple signal measurements, they can offer reduced sensitivity to partial volume effects. At the same time, however, these techniques require pulse sequence modifications and multiple echoes or acquisitions that usually prolong scan times.

Phase-sensitive SSFP (PS-SSFP) is a scan-time-efficient alternative for fat–water separation that does not require modification of standard bSSFP sequences.[15] PS-SSFP generates out-of-phase fat and water signals by placing their respective resonances in neighboring bSSFP passbands. Following a correction for additional slow-varying phase components due to inadvertent factors such as field inhomogeneity and coil sensitivity, PS-SSFP leverages abrupt phase changes arising near fat–water boundaries to separate the two signals. However, residual phase variations that remain in corrected images can cause suboptimal fat–water separation.[16]

PS-SSFP reconstructions have been previously demonstrated to work reliably on images acquired with quadrature

View this article online at wileyonlinelibrary.com. DOI: 10.1002/jmri.25138

Received Oct 8, 2015, Accepted for publication Dec 8, 2015.

*Address reprint requests to: T.Ç., Department of Electrical and Electronics Engineering, Bilkent University, Ankara, TR-06800, Turkey. E-mail: cukur@ee.bilkent.edu.tr

From the [1]Department of Electrical and Electronics Engineering, Bilkent University, Ankara, Turkey; [2]National Magnetic Resonance Research Center, Bilkent University, Ankara, Turkey; and [3]Neuroscience Program, Bilkent University, Ankara, Turkey

coils.[15,16] Unlike quadrature coils with uniform coil sensitivity, individual channels in phased-array coils typically have relatively large spatial variations in sensitivity, resulting in increased noise while estimating image phase away from the coil centers. While an earlier study has proposed to address this issue by performing phase-sensitive reconstruction on a single combined image across coils,[17] intercoil inconsistencies in image phase may cause phase errors in the combination and deteriorate reconstruction performance. Other important studies have proposed performing separate phase-sensitive reconstructions on individual-coil images, which were then combined by aligning intercoil phase offsets to prevent fat–water swaps.[2,18] However, residual phase errors between individual-coil images may show complex spatial variations and thus may not fully correctable by global factors.

Here we propose and assess an improved strategy for phase-sensitive fat–water separation in bSSFP images acquired with phased-array coils. The specific aims of this study were to improve the accuracy of region-growing phase correction via an unsupervised seed-selection procedure, to enhance tissue classification by optimally aggregating phase information across individual-coil images, and finally to demonstrate the performance of the proposed strategy in vivo on bSSFP angiograms acquired in the lower extremities.

Materials and Methods

Dual-Acquisition PS-SSFP Reconstruction

The PS-SSFP approach relies on the frequency dependence of bSSFP magnetization profiles.[15] Balanced SSFP sequences generate periodic magnetization profiles, with π-radians phase difference between consecutive passbands (Fig. 1a). Therefore, a $\Delta\phi = \pi$ phase-cycled bSSFP sequence can produce out-of-phase images when the repetition time (TR) is selected to place fat and water resonances an odd number of passbands apart, $TR = (2n+1)/\Delta f$ where n is an integer and Δf is the fat–water frequency difference (eg, TR = 4.6 msec at 1.5T). To improve immunity against off-resonance while maintaining this phase difference, dual-acquisition PS-SSFP[16] acquires a separate $\Delta\phi = 0$ phase-cycled bSSFP image, and complex sums the $\Delta\phi = \pi$ and $\Delta\phi = 0$ images (Fig. 1a). The acquired signal can be expressed as:

$$S(r) = [W(r) - F(r)] \cdot e^{-i\theta(r)} \quad (1)$$

where r is the spatial location, W is the level of water signal, F is the level of fat signal, and Θ denotes the spatially varying image phase due to various sources including field inhomogeneity, susceptibility, and coil sensitivity.

PS-SSFP assumes that each voxel contains dominantly fat or water tissue, and that $\Theta(r)$ is distinguishable from the rapid phase shifts near fat–water boundaries. In such cases, a region-growing phase-correction can be applied to remove the slowly varying phase component, $\Theta(r)$.[2,14,15] In the current study, we use the correction algorithm proposed by Hargreaves et al.[16] This algorithm first splits the imaging volume into small blocks (eg, $6 \times 6 \times 6$ voxels). Starting with a seed block, it updates the block phases by π-radians when necessary, such that the intensity-weighted sum of block phases varies smoothly across the image. Following correction of the images for the estimated block phases, phase-sensitive fat–water separation is performed.

The reliability of PS-SSFP can be compromised by rapid phase variations that violate the assumption of gradually varying $\Theta(r)$. Unlike quadrature coils with broad spatial coverage, phased-array coils typically introduce large phase variations away from the coil centers where the individual-coil sensitivity diminishes. To demonstrate typical differences in image phase between quadrature-coil and phased-array data, we acquired bSSFP images of the lower leg with TR = 9.2 msec at 1.5T using both a quadrature coil and a receive-only 8-channel phased-array coil. This TR selection—an even multiple of the ideal TR—places fat and water resonances two passbands apart, and thus the resulting tissue signals are in phase. The distributions of voxel magnitude and phase across in-phase bSSFP images were visualized (Fig. 1b). As expected, voxel phases are much more broadly spread and variable in a phased-array coil compared to a quadrature-coil. These excessive phase variations in turn increase the possibility of fat–water misclassification in phased-array bSSFP acquisitions.

PS-SSFP for Phased-Array Acquisitions

We propose a strategy to improve phase-sensitive reconstructions of bSSFP data acquired with phased-array coils. In regular PS-SSFP, a central voxel is selected as the starting seed for region-growing phase correction.[15] A single, common seed can be designated for all coils to prevent global phase inconsistencies among coils.[2] However, in coils for which the starting seed is relatively distant to the peak sensitivity region, this procedure can cause suboptimal phase correction and fat–water swaps in subsequent reconstructions. To address this issue, we propose an unsupervised technique for coil-wise seed selection (Fig. 2a). This technique first reconstructs a low-resolution image for each coil by Fourier transforming the central 4% of *k*-space data. The coil-sensitivity profiles ($C_{1,\ldots,N}$) are then taken as the ratio of these individual-coil images to the sum-of-squares combination of low-resolution images across coils.[19] Note that fat typically yields much higher bSSFP signals than water tissues in the lower extremities considered here.[20] A fat-voxel seed can thus be selected based on signal intensity. However, since tissue boundaries may be blurred in low-resolution sensitivity profiles, the sensitivity peak may correspond to a water or background voxel neighboring a high-intensity fat voxel. For this reason, the sensitivity profile is multiplied with the magnitude of the respective full-resolution coil image prior to selection. The voxel that maximizes this product is then designated as the seed for each coil. This procedure ensures that seeds are in close proximity to the sensitivity peaks.

Next, we employ a separate region-growing phase correction on each coil with the previously identified seeds to remove the slowly varying phase components (Fig. 2b). We initiate the phase correction in each coil on a high-signal fat voxel. As a result, fat voxels in corrected coil images will tend to cumulate around 0 radians (positive real part), whereas water voxels will cumulate around π-radians (negative real part).[15] This seed-selection procedure thereby accounts for intercoil phase offsets, avoiding global

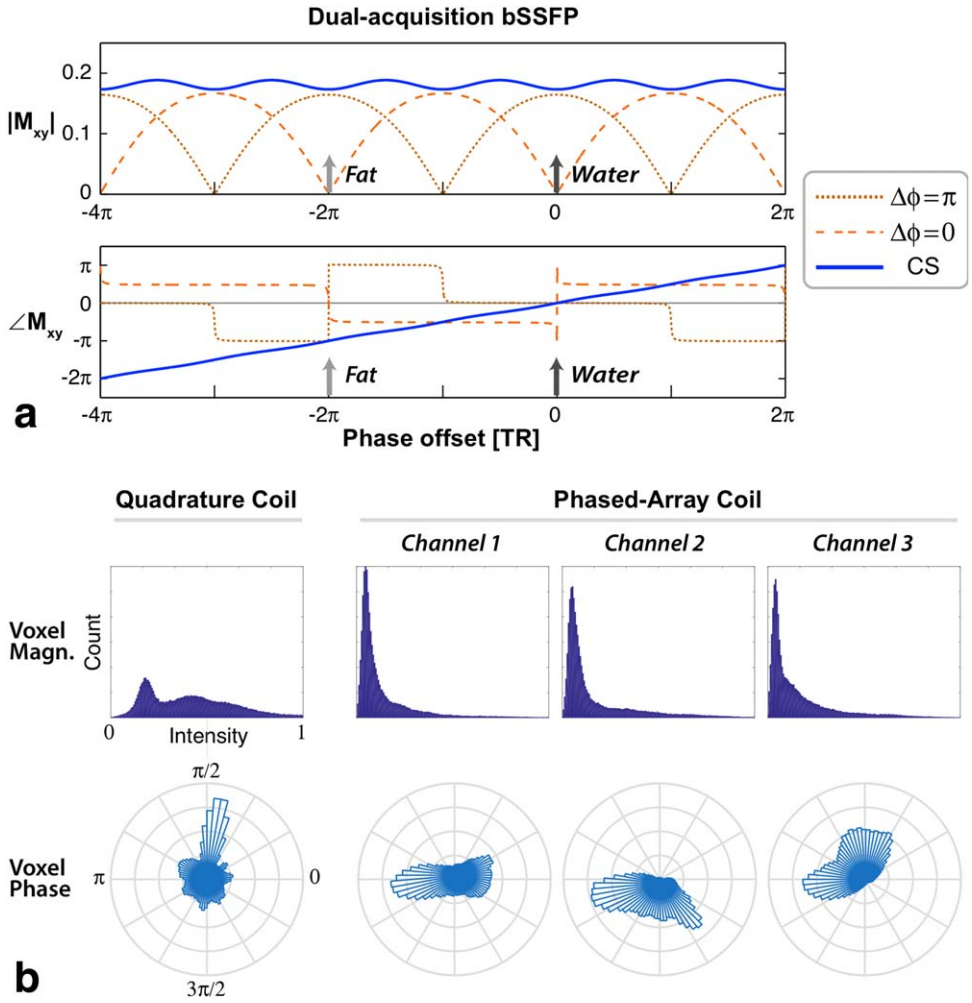

FIGURE 1: (a) Transverse magnetization profiles of $\Delta\phi = \pi$ (dotted line) and $\Delta\phi = 0$ (dashed line) phase-cycled bSSFP sequences were simulated along with their complex-sum (CS, solid line). The simulations assumed 90° flip angle, TR/TE = 4.6/2.3 msec and T_1/T_2 = 1200/250 msec at 1.5T. Magnitude (top row) and phase (bottom row) profiles are shown separately, and the locations of fat and water resonances are marked with arrows. Fat and water signals are π-radians out of phase for $\Delta\phi = \pi$ but large field inhomogeneity may cause water or fat resonances to leak into neighboring bands. CS maintains the π-radians fat–water phase difference while reducing sensitivity to field inhomogeneity. (b) To detect this phase difference, PS-SSFP uses a correction step to remove phase variations from additional sources including coil sensitivity. To illustrate the effects of coil sensitivity, in-phase bSSFP images (TR/TE = 9.2/4.6 msec at 1.5T) were acquired using a quadrature extremity coil and an 8-channel phased-array coil (three representative channels are shown). Histograms of voxel magnitude (top row) and polar histograms of voxel phase (bottom row) are visualized. Because individual channels in the phased-array coil have compact spatial coverage, voxel magnitudes accumulate around lower intensities compared to the quadrature-coil image. The narrow sensitivity profiles also cause the voxel phases to be more broadly spread in phased-array images.

fat–water swaps across separate coils. However, correction accuracy can still degrade in regions away from the coil center where reduced coil sensitivity yields low image magnitude and noisy phase. Therefore, we propose to obtain accurate phase estimates by pooling information across coils. Here we assume that the coil elements in the phased array collectively provide sensitive coverage across the entire imaging field of view (FOV). The following linear combination of coil images can then be computed[19]:

$$S_{cmb}(r) = \frac{\sum_{i=1}^{N} S_i^{pc}(r) \cdot |C_i(r)|}{\sum_{i=1}^{N} |C_i(r)|} \qquad (2)$$

where S_i^{pc} denotes the phase-corrected image from the ith coil, and N is the number of coils. Note that the coil-sensitivity profiles estimated from central *k*-space data contain residual image phase. To prevent intercoil inconsistencies due to this remnant phase, the phase-corrected coil images in Eq. 2 are weighted by the magnitude of coil sensitivities. Finally, the phase of S_{cmb} is used to classify each voxel as water or fat.

Alternative PS-SSFP Reconstructions

To compare the performance of the proposed multiseed combined-coil method, we implemented three alternative PS-SSFP reconstructions:

1. Single-seed individual-coil reconstruction (PS_{ss}): In PS_{ss}, a fat voxel centrally located within the volume was selected manually as a common seed for all coils. Phase correction was performed individually on each coil image starting with this common seed. Following phase correction, global phase offsets among

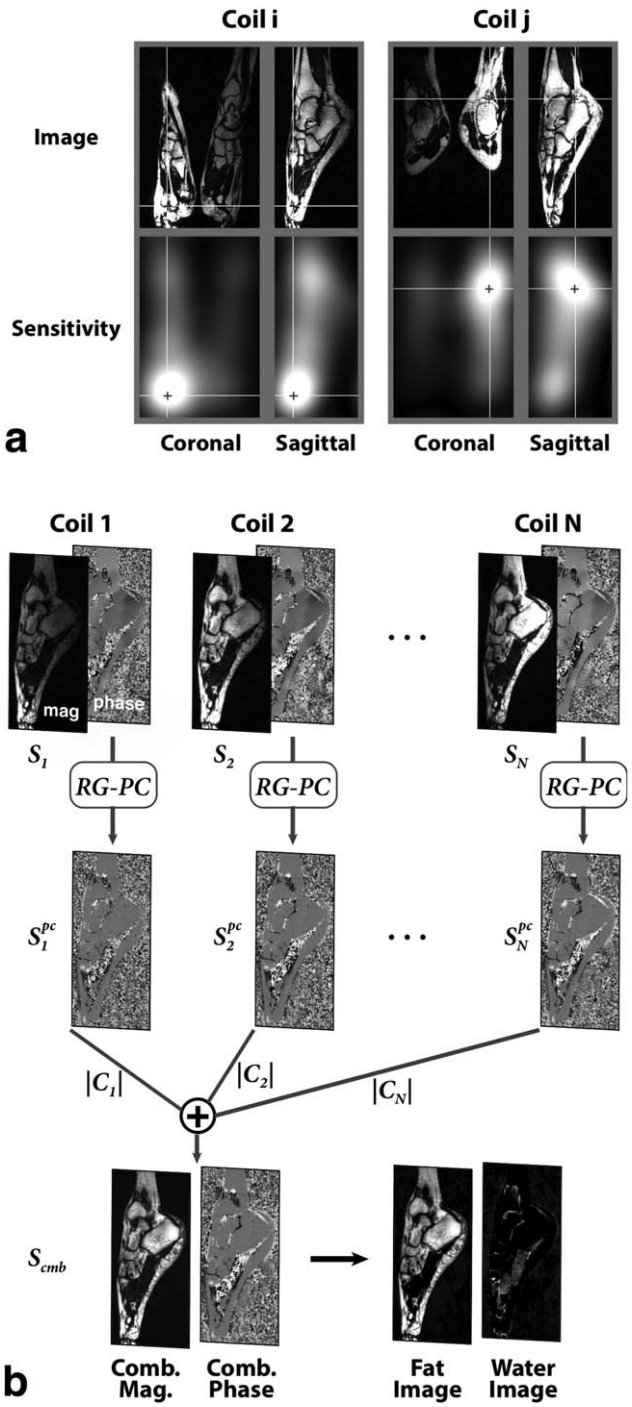

FIGURE 2: The proposed method. (a) The initial step of the proposed reconstruction is to identify fat-voxel seeds near the peak of each coil's sensitivity profile. To do this, sensitivity maps are first estimated from the central portion of *k*-space data for each coil (bottom row). These maps are then multiplied with the corresponding bSSFP images (top row), and for each coil the voxel that maximizes the product is selected as the starting seed (marked with blue crosses). (b) Following coil-wise seed selection, region-growing phase correction (RG-PC) is applied to individual-coil images (S_i) in order to remove slowly varying phase components. The phase-corrected coil images (S_i^{PC}) are then linearly combined, where images are weighted by the magnitude of respective coil sensitivities ($|C_i|$). Phase-sensitive fat–water separation is finally performed based on the magnitude and phase of the combined image (S_{cmb}).

coil images were removed, and individual-coil water images were reconstructed.[2,18] The final reconstruction was calculated as a weighted combination of individual-coil water images, where each coil's weight was proportional to the magnitude of its sensitivity, as in Eq. 2.

2. Multiseed individual-coil reconstruction (PS_{ms}): In PS_{ms}, the starting seeds were determined according to the unsupervised selection procedure employed in the proposed method. The remaining parts of PS_{ms} were identical to the PS_{ss} reconstruction. Thus, water images were reconstructed separately for each coil and then linearly combined.
3. Single-seed combined-coil reconstruction (PS_{cc}): The first step of PS_{cc} was to calculate a linear combination of coil images[19]:

$$S_{cc}(r) = \frac{\sum_{i=1}^{N} S_i(r) \cdot C_i^*(r)}{\sum_{i=1}^{N} |C_i(r)|} \qquad (3)$$

where uncorrected coil images S_i are multiplied with the complex conjugate of the coil sensitivities C_i^*. Note that weighting uncorrected coil images by the sensitivity magnitudes as in Eq. 2 would cause signal loss due to intercoil phase inconsistencies. Instead, the combination in Eq. 3 removes from individual-coil images the low-spatial-frequency phase variations captured by the sensitivity estimates (including global phase terms). To account for gradual phase variations still remaining in the combination, region-growing phase correction was performed on S_{cc} using a central fat-voxel seed, and the resulting phase-corrected image was used for fat–water separation.

Experiments

Noncontrast-enhanced bSSFP angiograms were acquired at three separate stations in the lower extremities: the thigh, the calf, and the foot. Data were collected on a 1.5T GE (Milwaukee, WI) Signa scanner (40 mT/m maximum strength, 150/T/m.s maximum slew rate) using an 8-channel receive-only phased-array coil. Three volunteers were recruited for the study (two females ages 28 and 34, one male age 28), and all subjects gave written informed consent. The experimental protocols were approved by the local Institutional Review Board.

To generate angiographic contrast, we used a magnetization-prepared, segmented 3DFT bSSFP sequence that we developed in a recent study.[21] Dual-acquisition bSSFP data were acquired and complex summed to mitigate banding artifacts due to field inhomogeneity.[16] The following parameters were prescribed: superior–inferior readout direction, 90° flip angle, 5 msec TR (the minimum TR allowed by the readout requirements), 2.5 msec TE, 1.7 seconds inversion recovery time, 80 msec T_2-preparation time, 1200 encodes/segment, 12-tip start-up catalyzation based on a Kaiser-Bessel windowed ramp, and 3 seconds recovery time. A relatively high flip angle was prescribed to increase suppression of muscle signal due to on-resonant magnetization transfer effects. In the thigh, an FOV of $350 \times 350 \times 180\,mm^3$ was covered with 1.4 mm isotropic resolution in 7 minutes 25 seconds. In the calf, an FOV of $310 \times 240 \times 140\,mm^3$ was covered with 1 mm isotropic resolution in 7 minutes 46 seconds. In the foot, an FOV of

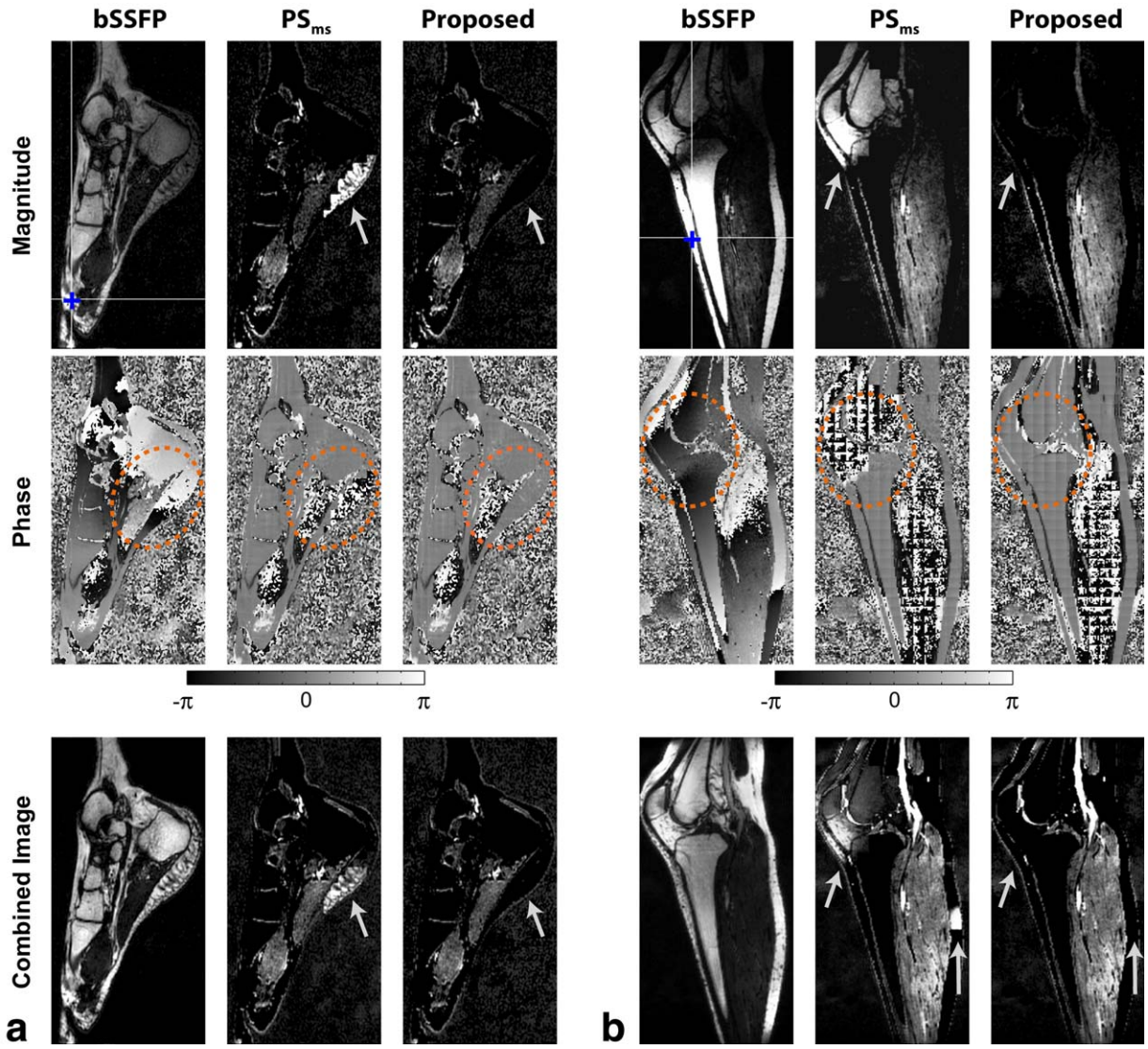

FIGURE 3: Dual-acquisition bSSFP images in the lower extremities, the foot (a) and the lower leg (b), collected using an 8-channel phased-array coil. Unseparated complex-sum images are shown for bSSFP, whereas water images are shown for PS_{ms} (multiseed, individual coil) and the proposed method. Note that PS_{ms} was performed individually on each coil, and seed selection was identical across the two methods (starting seeds marked with blue crosses). In both a and b, the top row shows magnitude images and the middle row shows phase images (see colorbar) obtained from an individual coil. Meanwhile, the bottom row shows the final image combined across coils. Relatively large variations are observed in phase images away from the sensitivity peak of the coils: in posterior regions of the foot image and superior–anterior regions of the lower leg (marked with dashed ellipses). While these variations cause fat–water misclassification in individual-coil and combined PS_{ms} images (marked with arrows), the proposed method produces more reliable phase estimates to improve tissue classification.

$270 \times 200 \times 140\,mm^3$ was covered with 1 mm isotropic resolution in a total scan time of 6 minutes 28 seconds. All PS-SSFP reconstructions were performed using a block of size $6 \times 6 \times 6$ voxels. Prior to maximum-intensity projections (MIPs), all datasets were transformed to *k*-space, zero-padded to double the *k*-space coverage, and inverse Fourier-transformed. This procedure was performed to minimize partial volume effects and to improve visualization quality.[22]

As a reference for PS-SSFP reconstructions, IDEAL (Iterative Decomposition of Water and Fat with Echo Asymmetry and Least-Squares Estimation) fat–water separation was implemented on dual-acquisition bSSFP data separately collected using a multiecho bipolar-readout 3DFT sequence.[23] The IDEAL sequence was implemented using TR = 10 msec and three echoes with 2.8-msec spacing, TE = (1.3, 4.1, 6.9) msec. To maintain identical spatial resolution, FOV, and scan time to PS-SSFP acquisitions at each station, IDEAL acquisitions were 1.5-fold accelerated and undersampled data were reconstructed using ARC (Autocalibrating Reconstruction for Cartesian Sampling).[24] A multipeak IDEAL reconstruction was then performed to separate fat and water signals.[25]

Two complementary analyses were performed to evaluate PS-SSFP reconstructions. First, PS-SSFP water images were compared with unseparated bSSFP images. PS-SSFP classifies each voxel as either water or fat. It has been reported in the lower extremities at 1.5T that the average intensity of fat signals is at least twice as high as the average intensity of water signals.[20] Thus, the intensity

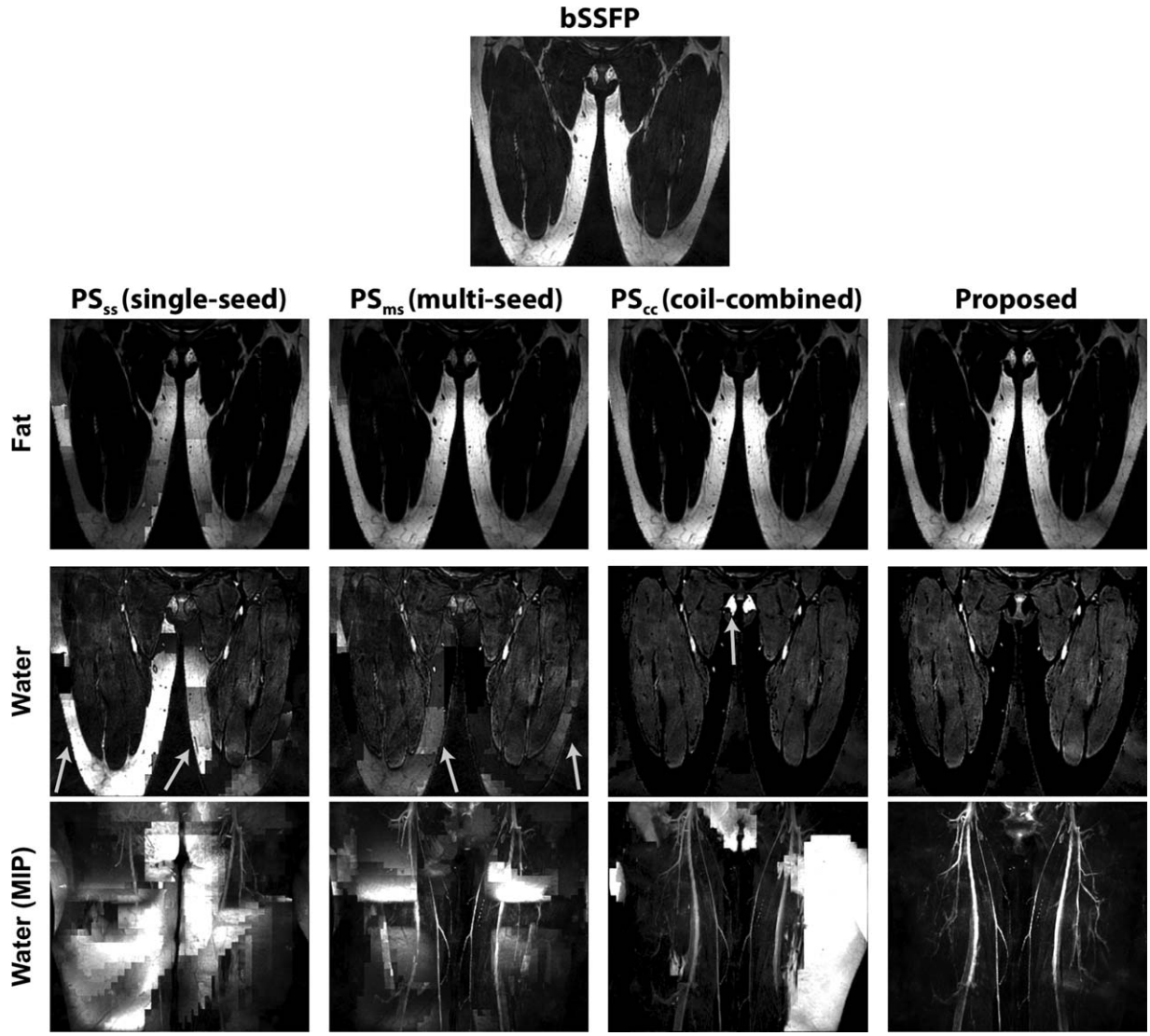

FIGURE 4: In vivo thigh images combined across 8 channels of a phased-array coil. First row: The unseparated bSSFP image shown as a reference. Second row: A coronal slice from fat images reconstructed using PS_{ss}, PS_{ms}, PS_{cc}, and the proposed method. Third row: A coronal slice from water images reconstructed using PS_{ss}, PS_{ms}, PS_{cc}, and the proposed method. Fourth row: Maximum-intensity projections (MIPs) across water images. Residual fat signals are seen in multiple regions of regular PS-SSFP reconstructions (marked with arrows). In contrast, the proposed method maintains reliable fat–water separation across the imaging volume.

of PS-SSFP water images should become smaller with improved fat suppression. To compare the level of fat suppression across different PS-SSFP methods, we measured the mean image intensity across axial cross-sections of each reconstruction. In each cross-section we calculated the ratio of the mean intensities measured in PS-SSFP versus bSSFP images (R_{bSSFP}; expected to decrease with improved fat suppression).

It is possible that misclassification of water tissue that yield higher bSSFP signals than fat (eg, synovial fluid) can introduce a downward bias in the intensity ratio of PS-SSFP to unseparated bSSFP images. To ensure that these ratio measurements are not significantly biased by suboptimal water signals, a separate control analysis was performed. In this analysis, PS-SSFP and IDEAL water images were compared after intensity normalization. For normalization, an identical region-of-interest (ROI) with homogeneous muscle signal (minimum size of 500 voxels) was selected across all reconstructed volumes. The mean signal intensity within the muscle ROI was normalized to unity separately for PS-SSFP and IDEAL images. PS-SSFP images with more reliable fat–water separation should yield similar intensities to the reference IDEAL images. In each axial cross-section, we calculated the ratio of the mean intensities measured in PS-SSFP versus IDEAL images (R_{IDEAL}; expected to approach 1 with improved water signals). All statistical comparisons were performed using Wilcoxon signed-rank tests ($P < 0.005$).

Results

Balanced SSFP images of the foot and the lower leg from a sample coil, and corresponding water images reconstructed via PS_{ms} (multiseed, individual-coil) and the proposed method, are displayed in Fig. 3. The phase images become progressively noisier away from the sensitivity peak for each coil. Increased phase noise in turn causes local failures

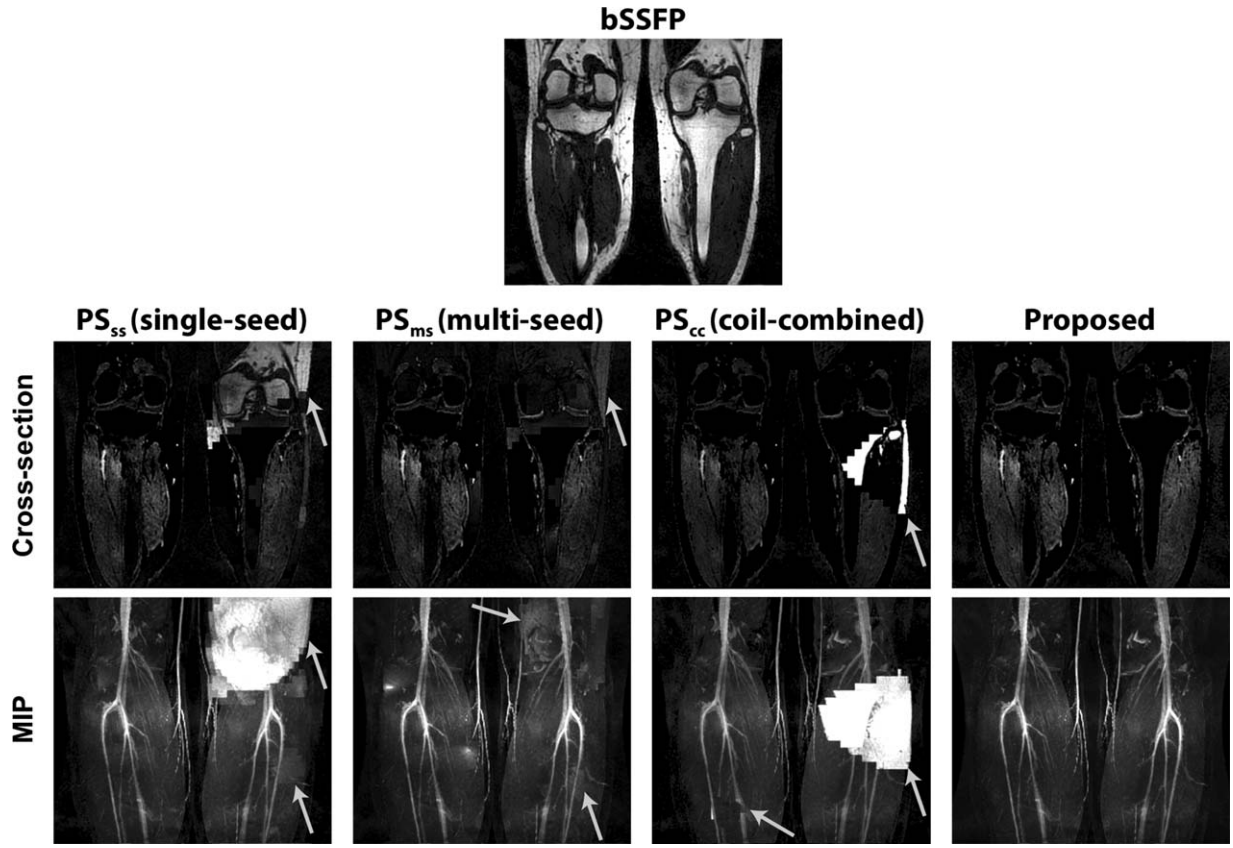

FIGURE 5: In vivo lower leg images combined across 8 channels of a phased-array coil. First row: The unseparated bSSFP image shown as a reference. Second row: A coronal slice from water images reconstructed using PS_{ss}, PS_{ms}, PS_{cc}, and the proposed method. Third row: MIPs across water images. Fat–water misclassification is seen broadly across regular PS-SSFP reconstructions (marked with arrows). Meanwhile, the proposed method achieves improved fat–water separation across the entire imaging volume.

during phase correction, and regional fat–water misclassification in PS_{ms}. Note that residual fat signals in individual-coil images are prominent even after image combination across coils. In contrast, the proposed method achieves visibly improved fat suppression compared to PS_{ms}.

Representative bSSFP images of the thigh and the lower leg reconstructed via PS_{ss} (single-seed, individual-coil), PS_{ms}, and PS_{cc} (combined-coil) are shown in Figs. 4 and 5. Both cross-sectional and MIP views of water images—combined across 8 channels of the phased-array coil—show broad regions of fat–water misclassification in PS_{ss}, PS_{ms}, and PS_{cc}. The combination across coils prior to phase correction in PS_{cc} and the coil-wise seed selection in PS_{ms} partly improve water depiction compared to regular PS_{ss}. Nonetheless, water images obtained via the proposed method demonstrate enhanced tissue separation compared to PS_{cc} and PS_{ms}.

Quantitative assessments of the level of fat suppression (R_{bSSFP}) and the optimality of water signals (R_{IDEAL}) are listed in Table 1. Our proposed method yielded significantly smaller R_{bSSFP} than each of the three alternative PS-SSFP reconstructions in the thigh, in the lower leg, and in the foot ($P < 0.005$), indicating that it achieves improved fat suppression. Furthermore, the proposed method attains the most similar image intensities to IDEAL (Fig. 6) among all PS-SSFP reconstructions in all body regions ($P < 0.005$). These results indicate that the proposed method achieves significantly more reliable fat–water separation compared to regular PS-SSFP reconstructions.

Discussion

PS-SSFP fat–water separation employs a correction algorithm to remove phase variations due to undesirable factors including coil sensitivity. This correction proves challenging in phased-array acquisitions since individual-coil image phase typically shows substantial variations away from the coil centers. The proposed method first uses a coil-wise seed selection for individual-coil phase correction and obtains accurate phase estimates near coil-sensitivity peaks. Phase-corrected images are then linearly combined to improve phase estimates in the remaining regions, thereby obtaining enhanced phase estimates across the imaging volume.

A number of effective techniques have been previously proposed for tissue separation in bSSFP imaging.[26] Sequences that employ saturation or spectral-spatial pulses for fat suppression can reduce sensitivity to partial volume effects and

TABLE 1. Quantitative Assessments of Fat-Water Separation

		PS_{ss}	PS_{ms}	PS_{cc}	Proposed
R_{bSSFP}	Thigh	0.363 ± 0.033	0.242 ± 0.044	0.252 ± 0.042	0.181 ± 0.039[a]
	Lower leg	0.290 ± 0.053	0.269 ± 0.072	0.267 ± 0.088	0.246 ± 0.089[a]
	Foot	0.176 ± 0.046	0.174 ± 0.049	0.176 ± 0.051	0.167 ± 0.048[a]
R_{IDEAL}	Thigh	2.163 ± 0.555	1.346 ± 0.184	1.485 ± 0.449	1.052 ± 0.213[a]
	Lower leg	1.766 ± 0.493	1.586 ± 0.377	1.623 ± 0.747	1.416 ± 0.403[a]
	Foot	1.685 ± 0.724	1.725 ± 0.782	1.729 ± 0.748	1.670 ± 0.796[a]

Measurements are reported as mean ± SD across cross-sections.
[a]Significantly different results ($P < 0.005$).

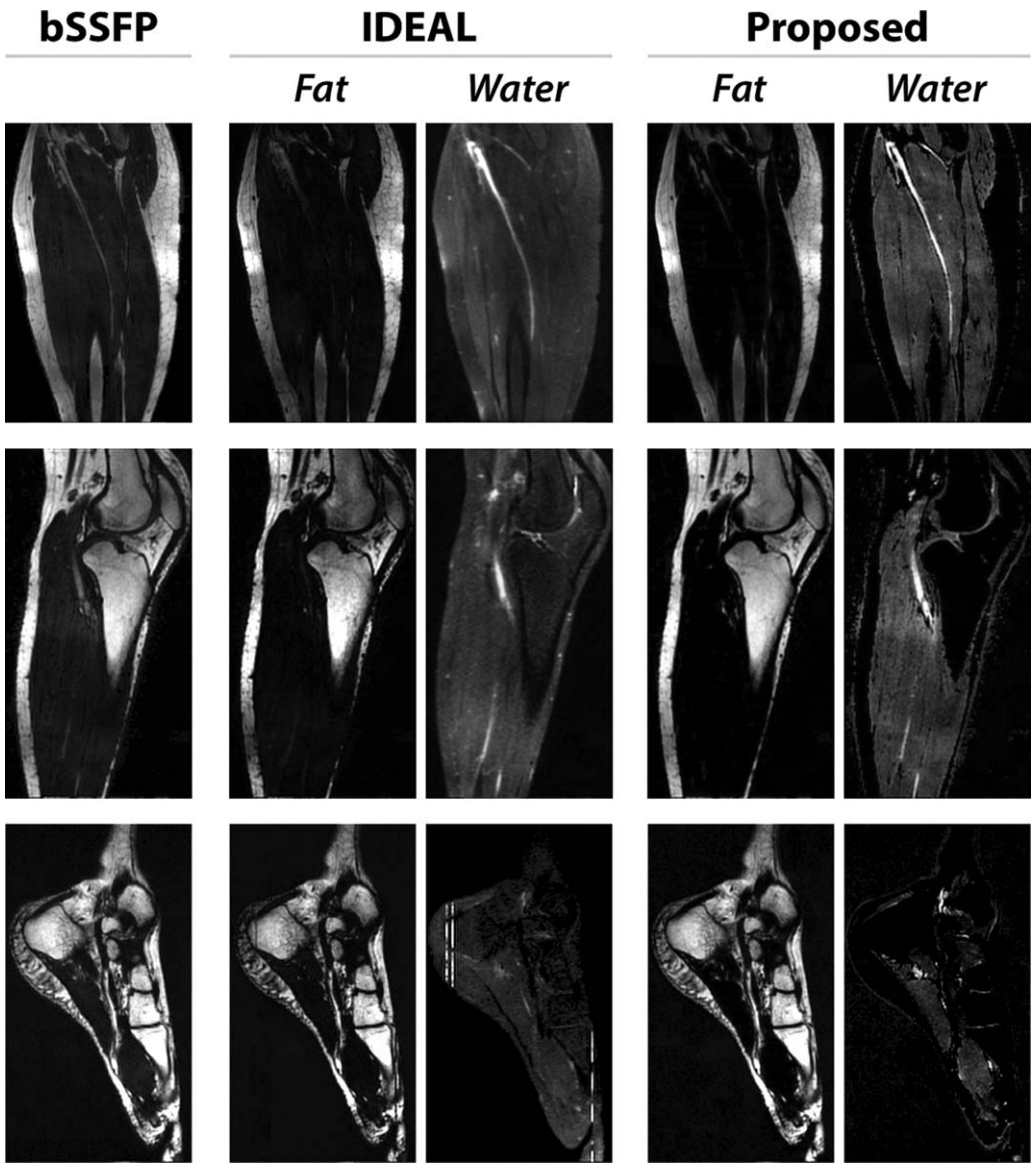

FIGURE 6: Unseparated bSSFP images, fat/water images reconstructed using IDEAL, and fat/water images reconstructed using the proposed method. First row: A sagittal slice from in vivo thigh images. Second row: A sagittal slice from in vivo lower leg images. Third row: A sagittal slice from in vivo foot images.

chemical-shift artifacts. Yet because these pulses reduce scan efficiency and increase sensitivity to field inhomogeneity, they are often not preferred in imaging extremities.[26] Meanwhile, Dixon-type methods including IDEAL use multiecho measurements to offer accurate quantification of subvoxel fat–water composition and improved immunity against field inhomogeneity. However, these methods require significantly prolonged scan times and complex reconstruction procedures. In contrast, PS-SSFP does not use special pulses, multiple echoes, or other sequence modifications. It separates fat and water based on a relatively simple phase-sensitive reconstruction, at the expense of increased sensitivity to partial volume effects. Therefore, the proposed method can offer fat–water separation with high scan and processing efficiency.

The application of PS-SSFP on phased-array acquisitions has been considered in several recent studies.[2,17] One approach is to first form a linear-combination image across coils, and then to perform fat–water separation on the combination.[17] This approach, related to PS_{cc}, can suffer from residual phase errors in the combined image due to inconsistencies of uncorrected image phase across individual coils. Alternatively, fat–water separation can be performed on individual-coil images as in PS_{ss} and PS_{ms}.[2] Images are then combined after correcting for global phase offsets among separate coils.[18] However complex, intercoil phase inconsistencies may exist even after coil-wise phase correction. The proposed method comprises several technical advances to achieve improved fat–water separation compared to previous approaches. Unlike PS_{cc}, our method performs phase correction prior to image combination across coils. In this process, it utilizes an automated selection to place seeds in regions of high coil sensitivity as opposed to a common seed for all coils. Finally, unlike PS_{ss} or PS_{ms}, it separates fat–water voxels based on an improved phase estimate obtained via combination of corrected coil images.

A basic limitation of PS-SSFP concerns the selection of the sequence TR. A TR of 4.6 msec at 1.5T (or 2.3 msec at 3T) ideally places fat and water resonances at the centers of adjacent passbands. While out-of-phase images can be acquired at odd multiples of the ideal TR (eg, TR = 6.9 msec at 3T), these longer TRs may be undesirable since they increase field-inhomogeneity induced phase variations. However, TR = 6.9 msec or longer could be required for 3T imaging where the ideal TR is too restricted to maintain practical readout resolutions. Therefore, PS-SSFP at higher field strengths can offer improved signal-to-noise ratio (SNR) while increasing sensitivity to field inhomogeneity. It is also possible to prescribe moderately longer/shorter TRs than the ideal value (eg, TR = 5 msec at 1.5T was the minimum possible TR in this study). Such alterations cause the fat resonance to be offset from the passband center, slightly perturbing the fat–water phase difference in dual-acquisition bSSFP. Because PS-SSFP assumes a π-radians fat–water phase difference, accurate tissue classification is expected when the total phase accrual due to chemical shift and field inhomogeneity is less than $\pi/2$-radians. Thus, TR perturbations that increase chemical-shift induced phase effectively reduce the tolerable range of field inhomogeneity.

The proposed method has some other technical limitations that are common to PS-SSFP reconstructions. First, the current implementation comprises two sequential phase-cycled acquisitions, increasing susceptibility to motion. To mitigate artifacts due to patient motion, retrospective motion correction can be performed using navigators incorporated into bSSFP sequences. Second, PS-SSFP classifies each voxel as either fat or water, introducing sensitivity to partial volume effects. Spatial resolution can be increased to reduce this sensitivity, while undersampling can be used to maintain scan-time efficiency. Lastly, when field inhomogeneity is significant, residual banding artifacts might be visible in dual-acquisition bSSFP images. To improve robustness against field inhomogeneity, the proposed method can be applied to complex-sum images from a greater number of phase-cycled acquisitions without any modification.

Several technical developments can be further considered to improve the proposed fat–water separation. While PS-SSFP assumes a single-peak model for the fat resonance, a multipeak extension could offer enhanced tissue delineation.[25] Note that a multipeak model based on single-echo acquisitions would be underconstrained. However, a dual-echo acquisition may enable subvoxel tissue decomposition, assuming that the parameters of the fat spectrum are calibrated a priori.[27] Another improvement concerns the phase correction step of the proposed method. We preferred a region-growing algorithm[2,15,16] in this study because it yielded high-quality reconstructions in the lower extremities, and it offered computationally efficient reconstructions for three-dimensional datasets. However, iterative phase-correction algorithms based on graph cuts can further improve reliability against large field inhomogeneities.[27]

The proposed fat–water separation method was demonstrated successfully for noncontrast-enhanced angiograms acquired in three body parts in the lower extremities. Although a relatively small number of healthy subjects is reported, these promising results motivate a more direct examination of the reliability of our method under clinical settings. In particular, future studies are warranted that consider a larger population, including patients with vascular disease, various other body parts and habitus, reproducibility assessments, and validation.

In conclusion, we have demonstrated improved phase-sensitive reconstructions of phased-array images, by combining an unsupervised seed-selection procedure for region-growing phase correction and an optimal pooling of phase information across coils. Thus, the proposed method is a promising technique for rapid fat–water separation in bSSFP applications.

Acknowledgments

Contract grant sponsor: European Molecular Biology Organization; contract grant number: Installation Grant (IG 3028); a TÜBITAK 3501 Career Grant (114E546); a TÜBITAK 2232 Fellowship (113C011); a Marie Curie Actions Career Integration Grant (PCIG13-GA-2013-618101); TÜBA GEBIP 2015 fellowships awarded to T. Çukur and E.U. Saritas

We thank Brian Hargreaves, Jean Brittain, Ann Shimakawa, Huanzhou Yu, and Dwight Nishimura for help with various aspects of this research.

Conflict of Interest

The authors declare no conflicts of interest.

References

1. Bieri O, Mamisch TC, Trattnig S, Kraff O, Ladd ME, Scheffler K. Optimized spectrally selective steady-state free precession sequences for cartilage imaging at ultra-high fields. MAGMA 2008;21:87–94.
2. Wansapura JP. Abdominal fat–water separation with SSFP at 3 Tesla. Pediatr Radiol 2007;37:69–73.
3. Cukur T, Lee JH, Bangerter NK, Hargreaves BA, Nishimura DG. Non-contrast-enhanced flow-independent peripheral MR angiography with balanced SSFP. Magn Reson Med 2009;61:1533–1539.
4. Lu A, Grist TM, Block WF. Fat/water separation in single acquisition steady-state free precession using multiple echo radial trajectories. Magn Reson Med 2005;54:1051–1057.
5. Leupold J, Hennig J, Scheffler K. Alternating repetition time balanced steady state free precession. Magn Reson Med 2006;55:557–565.
6. Cukur T, Nishimura DG. Multiple repetition time balanced steady-state free precession imaging. Magn Reson Med 2009;62:193–204.
7. Absil J, Denolin V, Metens T. Fat attenuation using a dual steady-state balanced-SSFP sequence with periodically variable flip angles. Magn Reson Med 2006;55:343–351.
8. Scheffler K, Heid O, Hennig J. Magnetization preparation during the steady state: fat-saturated 3D TrueFISP. Magn Reson Med 2001;45:1075–1080.
9. Paul D, Hennig J, Zaitsev M. Intrinsic fat suppression in TIDE balanced steady-state free precession imaging. Magn Reson Med 2006;56:1328–1335.
10. Derbyshire JA, Herzka DA, McVeigh ER. S5FP: spectrally selective suppression with steady state free precession. Magn Reson Med 2005;54:918–928.
11. Huang T-Y, Chung H-W, Wang F-N, Ko C-W, Chen C-Y. Fat and water separation in balanced steady-state free precession using the Dixon method. Magn Reson Med 2004;51:243–247.
12. Reeder SB, Markl M, Yu H, Hellinger JC, Herfkens RJ, Pelc NJ. Cardiac CINE imaging with IDEAL water-fat separation and steady-state free precession. J Magn Reson Imaging 2005;22:44–52.
13. Cukur T, Nishimura DG. Fat–water separation with alternating repetition time balanced SSFP. Magn Reson Med 2008;60:479–484.
14. Ma J. Breath-hold water and fat imaging using a dual-echo two-point Dixon technique with an efficient and robust phase-correction algorithm. Magn Reson Med 2004;52:415–419.
15. Hargreaves BA, Vasanawala SS, Nayak KS, Hu BS, Nishimura DG. Fat-suppressed steady-state free precession imaging using phase detection. Magn Reson Med 2003;50:210–213.
16. Hargreaves BA, Bangerter NK, Shimakawa A, Vasanawala SS, Brittain JH, Nishimura DG. Dual-acquisition phase-sensitive fat–water separation using balanced steady-state free precession. Magn Reson Imaging 2006;24:113–122.
17. Vasanawala SS, Hargreaves BA, Nishimura DG. Phase sensitive SSFP parallel imaging. In: Proc 12th Annual Meeting ISMRM, Kyoto; 2004. p 2253.
18. Ma J. Multislice and multicoil phase-sensitive inversion-recovery imaging. Magn Reson Med 2005;53:904–910.
19. Cukur T, Lustig M, Nishimura DG. Multiple-profile homogeneous image combination: application to phase-cycled SSFP and multicoil imaging. Magn Reson Med 2008;60:732–738.
20. Mazumdar A, Hargreaves BA, Han E, Brau A, Yu H, Brittain J. Automated Fat–water Identification in Phase Sensitive SSFP. In: Proc 13th Annual Meeting ISMRM, Miami; 2005. p 2307.
21. Cukur T, Shimakawa A, Yu H, et al. Magnetization-prepared IDEAL bSSFP: a flow-independent technique for noncontrast-enhanced peripheral angiography. J Magn Reson Imaging 2011;33:931–939.
22. Du YP, Parker DL, Davis WL, Cao G. Reduction of partial-volume artifacts with zero-filled interpolation in three-dimensional MR angiography. J Magn Reson Imaging 1994;4:733–741.
23. Lu W, Yu H, Shimakawa A, Alley M, Reeder SB, Hargreaves BA. Water-fat separation with bipolar multiecho sequences. Magn Reson Med 2008;60:198–209.
24. Brau ACS, Beatty PJ, Skare S, Bammer R. Comparison of reconstruction accuracy and efficiency among autocalibrating data-driven parallel imaging methods. Magn Reson Med 2008;59:382–395.
25. Yu H, Shimakawa A, McKenzie CA, Brodsky E, Brittain JH, Reeder SB. Multiecho water-fat separation and simultaneous R2* estimation with multifrequency fat spectrum modeling. Magn Reson Med 2008;60:1122–1134.
26. Bley TA, Wieben O, François CJ, Brittain JH, Reeder SB. Fat and water magnetic resonance imaging. J Magn Reson Imaging 2010;31:4–18.
27. Hernando D, Kellman P, Haldar JP, Liang Z-P. Robust water/fat separation in the presence of large field inhomogeneities using a graph cut algorithm. Magn Reson Med 2010;63:79–90.